3D Finite-element Method of Ground Motion Simulation

H.P. Ding, Y.Y. Yu, G.C. Luo & J. Liao
Suzhou University of Science and Technology , P.R China

SUMMARY:
If uniformity isotopic medium is assumed between rupture fault and the ground layer, and full space radiation of the dislocation source is regarded as the ground layer seismic incident wave, the ground motion would be simulated which is considered the rupture process by seismic response of soil using finite element method. The calculation model area can be reduced by this method, and also calculation efficiency is improved. By comparing the analytic solutions based on the dislocation theory with results of the FEM, this method is proved the calculation accuracy.

Keywords: rupture fault, dislocation source, ground motion numerical simulation, finite element method

INTRODUCTION

Recently, studies of wave propagation and strong-ground-motion simulation considering source process, wave-path and site effects have been given increasing attention (e.g., Miyatake, 1980; Frankel and Vidale, 1992; Frankel, 1993; Graves, 1993; Yomogida and Etgen, 1993; Olsen *et al.*, 1995; Olsen and Archuleta, 1996; Ohminato and Chouet, 1997; Pitarka *et al.*, 1998; Wald and Graves, 1998).

With respect to the simulation of source rupture process, equivalent load method based on moment tensor of dislocation source is widely applied, in which the dislocation is equivalent to double-couple loads which are then applied to the corresponding finite element nodes, and many efficient finite-difference algorithms are developed. When using this equivalent double-couple method, the rupture sources are generally embedded within the computation model, one of whose advantages is the ability to consider the reflection influence of crust layering structures under the source, but the computation region and amount are quite large. A long-period seismic motions simulation method was presented by Liu *et al.*(2008), who combines explicit finite-element method with parallel calculation technique. Neglecting the effect of crust structures of fault region on wave propagation, the fault region can be simplified to homogeneous medium, then full space radiation of the dislocation source is regarded as the incident wave and applied to the computational region. Compared with the former methods, the calculation region become quite small, and calculation amount can be reduced accordingly. In this article, the accuracy of the method proposed by Liu et al.(2008) is validated through comparisons between finite-element numerical solutions based on this method and analytical solutions of point source and dislocation source in full space based on the dislocation theory.

1. FULL SPACE RADIATION FIELD OF GENERAL SHEAR DISLOCATION SOURCES

In an isotropic, homogenous and elastic full space medium, neglecting the discontinuities of body-force and stress, the elastic displacement field caused by discontinuities across an internal surface $\sum$ of the fault can be expressed as follows:

$$u_n(x,t)=\iint_{\Sigma}[u_i(\xi,t)]l_j c_{ijkl}*G_{nk,l}(x,t;\xi,0)d\Sigma(\xi)=\iint_{\Sigma}m_{kl}*G_{nk,l}(x,t;\xi,0)d\Sigma(\xi) \quad (1.1)$$

where $[u_i(\xi,t)]$ is the source dislocation function, l_j represents normal on fault, c_{ijkl} is the constitutive relationship of fault medium, $m_{kl}=[u_i(\xi,t)]l_j c_{ijkl}$ is the seismic moment-density tensor .

Any displacement field caused by the dislocation on finite fault surface can be equivalent to contribution superposition of infinite point dislocation (the dislocation on the tiny area $d\Sigma(\xi)$), to a finite fault, the solution for shear point dislocation source can be expressed by the following equation:

$$du_n(x,t,\xi_1,\xi_2)=M_{pq}*G_{np,q}=u_n^N+u_n^{IP}+u_n^{IS}+u_n^{FP}+u_n^{FS} \quad (1.2)$$

Here,

$$u_n^N=\left(\frac{30\gamma_n\gamma_p\gamma_q v_q-6v_n\gamma_p-6\delta_{np}\gamma_q v_q}{4\pi\rho\, r^4}\right)\mu d\sum(\xi)\int_{r/\alpha}^{r/\beta}t'\Delta u_P(\xi_1,\xi_2,t-t')dt' \quad (1.3)$$

$$u_n^{IP}=\frac{12\gamma_n\gamma_p\gamma_q v_q-2v_n\gamma_p-2\delta_{np}\gamma_q v_q}{4\pi\rho\alpha^2 r^2}\mu d\sum(\xi)\Delta u_p(t-\frac{r}{\alpha}) \quad (1.4)$$

$$u_n^{IS}=-\frac{12\gamma_n\gamma_p\gamma_q v_q-3v_n\gamma_p-3\delta_{np}\gamma_q v_q}{4\pi\rho\beta^2 r^2}\mu d\sum(\xi)\Delta u_p(t-\frac{r}{\beta}) \quad (1.5)$$

$$u_n^{FP}=\frac{2\gamma_n\gamma_p\gamma_q v_q}{4\pi\rho\alpha^3 r}\mu d\sum(\xi)\Delta\dot{u}_p(t-\frac{r}{\alpha}) \quad (1.6)$$

$$u_n^{FS}=\frac{2\gamma_n\gamma_p\gamma_q v_q-v_n\gamma_p-\delta_{np}\gamma_q v_q}{4\pi\rho\beta^3 r}\mu d\sum(\xi)\Delta\dot{u}_p(t-\frac{r}{\beta}) \quad (1.7)$$

where u_n^N is the near-field coupling term, u_n^{IP}, u_n^{IS} are the intermediate-field P and S wave terms, u_n^{FP}, u_n^{FS} are the far-field P and S wave terms, respectively. Near-field coupling term u_n^N gains contributions from both P-wave potential gradient and S-wave potential rotation, and is composed of two motions of P-wave and S-wave. The physical meanings of parameters in the formulas can be found in Aki and Richards (1980), where $\alpha=\sqrt{\frac{\lambda+2\mu}{\rho}}$ represents the P-wave velocity, and $\beta=\sqrt{\frac{\mu}{\rho}}$ is the S-wave velocity.

Now there're several source time functions widely used, such as the Haskell function, the Bell function, and the exponent function, etc. Since long period motions are not sensitive to the specific dislocation process (Anderson and Richard, 1975), so the Bell function is used as the dislocation function in this article. To a finite fault, let $r(\xi)$ be the distance from point (ξ_1,ξ_2) on the fault to the initial rupture point, and v_r be the rupture velocity, then the dislocation at (ξ_1,ξ_2) can be expressed as follows:

$$\Delta u_p(\xi_1,\xi_2,t)=\begin{cases} 0 & t-r(\xi)/v_r<0 \\ \dfrac{D_p}{T}(t-r(\xi)/v_r-\dfrac{T}{2\pi}\sin\dfrac{2\pi}{T}(t-r(\xi)/v_r)) & 0\le t-r(\xi)/v_r<T \\ D_p & T\le t-r(\xi)/v_r \end{cases} \tag{1.8}$$

where T is the rise time, $\Delta u_p(\xi_1,\xi_2,t)$ denotes the dislocation for (ξ_1,ξ_2) in p direction (p=1,3), D_p denotes the final dislocation in p direction.

2. FINITE-ELEMENT CALCULATION METHOD

Finite-element numerical simulation method is used in this paper. The nodes of computational region can be divided into internal nodes and artificial boundary nodes, nodes at the artificial boundary are regarded as artificial boundary nodes, and the other nodes are all internal nodes, note that nodes at the free surface belong to the internal nodes. Based on explicit finite-element calculation, motion equations of all internal nodes can be expressed as follows:

$$\mathbf{M}\ddot{\mathbf{u}}+\mathbf{C}\dot{\mathbf{u}}+\mathbf{K}\mathbf{u}=\mathbf{P} \tag{2.1}$$

Here, ***M,C, K*** represent the matrixes of mass, damping, and stiffness, respectively, and ***P*** is the external force vector. For the calculation model in this article, ***P*** =**0**. By using the central-difference method, $\ddot{\mathbf{u}}$ can be approximately expressed in terms of the displacement components $\mathbf{u}$ as

$$\ddot{\mathbf{u}}^p=(\mathbf{u}^{p+1}-2\mathbf{u}^p+\mathbf{u}^{p-1})/\Delta t^2 \tag{2.2}$$

Using the explicit integration scheme combining central-difference with average approximation (Anderson and Richards, 1975), the recursion formulas of nodes displacements and velocities are

$$\mathbf{u}^{p+1}=(\mathbf{I}-\frac{1}{2}\Delta t^2\mathbf{M}^{-1}\mathbf{K})\mathbf{u}^p+(\mathbf{I}-\frac{1}{2}\Delta t\mathbf{M}^{-1}\mathbf{C})\Delta t\dot{\mathbf{u}}^p+\frac{1}{2}\Delta t^2\mathbf{M}^{-1}\mathbf{P}^p \tag{2.3}$$

$$\dot{\mathbf{u}}^{p+1}=\frac{2}{\Delta t}(\mathbf{u}^{p+1}-\mathbf{u}^p)-\dot{\mathbf{u}}^p \tag{2.4}$$

For artificial boundary nodes, the multi-transmitting boundary formulas (MTF, Liao ZP, 2002) are used

$$u_0^{p+1}=\sum_{j=1}^{N}(-1)^{j+1}C_j^N u_j^{p+1-j} \tag{2.5}$$

$$C_j^N=\frac{N!}{(N-j)!\,j!} \tag{2.6}$$

in which N denotes the order to be taken in MTF, 0 means boundary nodes, j represents internal nodes adjacent to 0.

It should be noted that in Eqn. 2.3, $\boldsymbol{u}$ is the displacements of full-wave field, while $\boldsymbol{u}$ in Eqn. 2.5 represents the displacements of scattered-wave field. To the bottom boundary of calculation model,

scattered-wave field displacements = full-wave field displacements – incident-wave field displacements; to the lateral boundary, since the calculation model used completely overlies the rupture surface, so there is no incident wave field, and scattered-wave field displacements = full-wave field displacements. Incident wave field displacements are acquired through analytical solutions of dislocation source in homogeneous isotropic elastic full space.

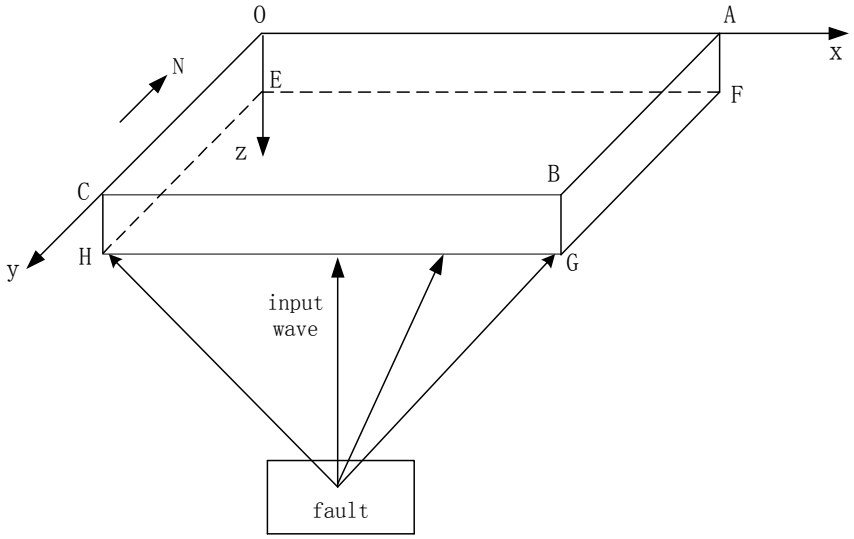

Figure 2.1. Finite-element computational model, OABC-EFGH represents the calculation region

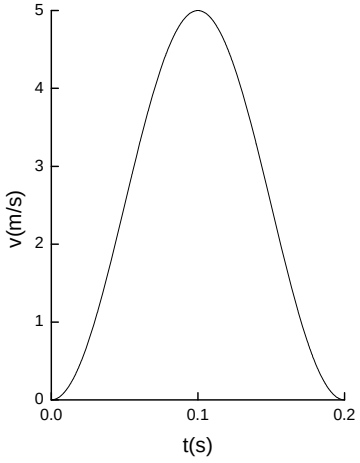

Figure 2.2. Source time function

3. COMPARISONS OF FINITE ELEMENT SOLUTIONS WITH ANALYTICAL SOLUTIONS FOR SHEAR DISLOCATION SOURCE

a) Comparisons of shear dislocation point source

The sizes of finite-element computation model (shown in Fig. 2.1) are: OB=OC=4.8km, OE= 0.75km, the calculation region is single elastic medium with shear wave velocity $v_s = 3km/s$, compression wave velocity $v_p = 3\sqrt{3}km/s$, density $\rho = 2000kg/m^3$, Poisson ratio $\gamma = 0.25$. The cube is adopted as finite element grid with space step $\Delta X = \Delta Y = \Delta Z = 15m$, and calculation time step $\Delta t = 0.002s$.

In order to obtain basic solution of point source ground motion, the Bell function is used as source time function in this paper, and the pulse width is 0.2 s (shown in Fig. 2.2). The source parameters are: fault strike $\varphi = 90^{\circ}$, dip angle $\delta = 90^{\circ}$, point dislocation rupture 0.2m, size of the point source 50m×50m, rupture point coordinate (2.415km, 2.43km, 4km).

Due to the disparities between P-wave and S-wave propagating velocities radiated from a point source, the reflected P-wave from the free surface will firstly be superposed with the incident S-wave inside the calculation region. For the convenience of studying wave propagation, the influence of near-field coupling term u_n^N is neglected in this paper, using P ($U_P = u_n^{IP} + u_n^{FP}$) and S ($U_S = u_n^{IS} + u_n^{FS}$) wave as the incident wave to finish the calculation separately, comparisons are made accordingly with P and S wave analytical solutions for homogeneous elastic full space. Three nodes' results are output with respective coordinates of No.1 (1.8km, 1.8km, 0.45km), No.2 (2.1km, 2.1km, 0.45km), No.3 (2.4km, 2.4km, 0.45km). The comparison results are shown as Fig. 3.1 and Fig. 3.2 respectively.

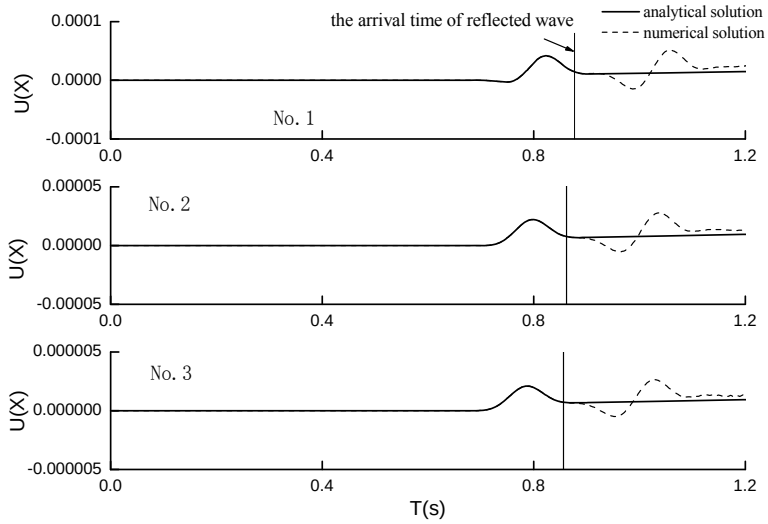

Figure 3.1. Comparison of X-component analytical and finite-element solutions for incident P-wave case of point source model

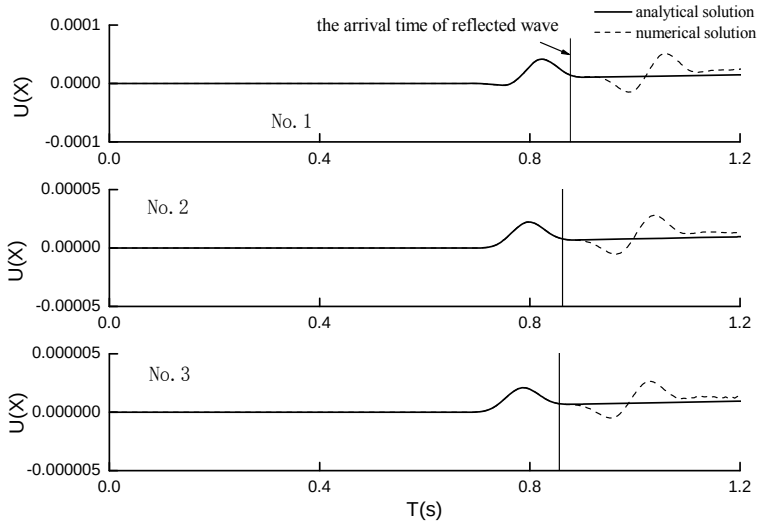

Figure 3.2. Comparison of X-component analytical and finite-element solutions for incident S-wave case of point source model

The solid line in Fig. 3.1 is P wave in homogeneous elastic full space, which can be viewed as analytical solutions for nodes to be output in the calculation model and can be obtained by Eqn. (1.4) and Eqn. (1.6). The solid line in Fig. 3.2 is S wave in homogeneous elastic full space, which can also be viewed as analytical solutions for nodes to be output in the calculation model and can be obtained by Eqn. (1.5) and Eqn. (1.7). The dashed lines in Fig. 3.1 and Fig. 3.2 denote corresponding finite-element numerical solutions. To both P and S wave, before the arrival of reflected wave, the finite-element solution can be regarded as the result of incident wave propagating in full space. It can be seen from Fig. 3.1 and Fig. 3.2 that the finite-element solutions are consistent with the analytical solutions before the arrival of reflected wave, demonstrating that the finite element method used in this article is right, and the accuracy is quite high.

b) Comparisons of dislocation line source

Let fault strike $\varphi = 90°$, dip angle $\theta = 90°$, dislocation equal to 0.2m (X direction), rise time equal to 0.2s, shear wave velocity $v_s = 3km/s$, compression wave velocity $v_p = 3\sqrt{3}km/s$, density $\rho = 2000kg/m^3$, Poisson ratio $\gamma = 0.25$. Coordinate of the southern end point near the free surface is (2.415km, 2.43km, 4.0km), and the initial rupture point (2.415km, 2.43km, 4.1km). The fault size is taken as 100m×200m with sub-fault size $\Delta L = \Delta W = 100m$, thus the fault surface is divided into two sub-faults. Rupture velocity of the fault is $v_r = 2.7km/s$. The finite-element calculation model is the same as the former point source case. Comparison results are shown in Fig. 3.3 and Fig. 3.4.

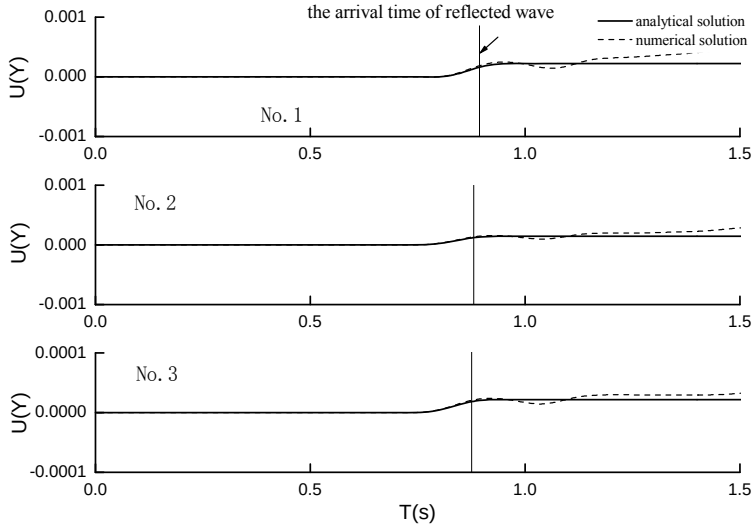

Figure 3.3. Comparison of Y-component analytical and finite-element solutions for incident P-wave case of line source model

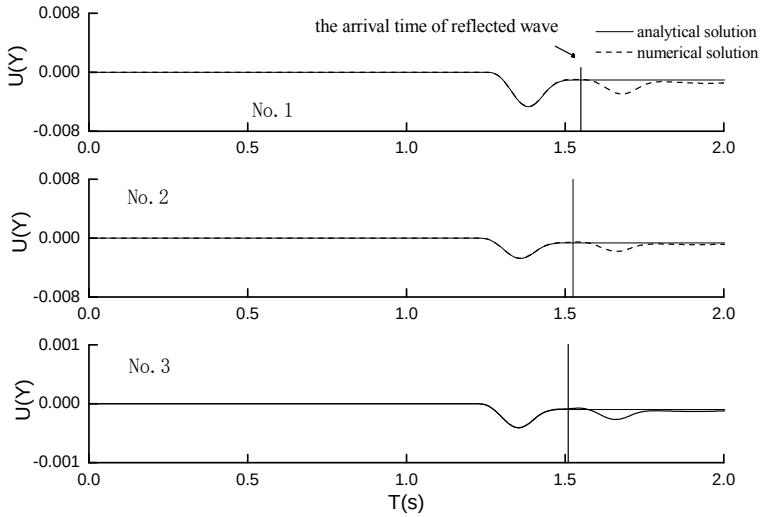

Figure 3.4. Comparison of Y-component analytical and finite-element solutions for incident S-wave case of line source model

It can be seen from Fig. 3.1-3.4 of comparisons between finite-element numerical solutions and corresponding analytical solutions that, before the arrival of reflected wave, the finite-element solution is consistent with the analytical solution.

4. CONCLUSIONS

Long-period ground motion finite-element simulation method (Liu et al., 2008) is used in this article, which assumes the crust structure between rupture fault and the ground layer is homogeneous medium. With waves radiated from dislocation source in full space as incident wave to the overburden layer bottom and use of finite element method to simulate the seismic response of overburden layer, the ground motion numerical simulation results can be gained which have considered the rupture process. Then the simulation results are compared with analytical solutions for homogeneous elastic full space based on dislocation theory, from the comparison results, it is shown that for internal nodes of the computational region, before the arrival of reflected wave, results of the two methods are completely same, demonstrating that the accuracy of the proposed finite element method can be guaranteed, and the method presented by Liu et al. (2008) is feasible. This method is suitable for the condition of uniform lower crust structure. Actually, since the exploration information of deep crust structure is not detailed enough in general, the above assumption is acceptable. Based on this premise, the proposed method has two primary strengths. First, for deep fault condition, it can significantly reduce the calculation model and then improve the efficiency, the requirements for computer hardware can be reduced as well. Second, the seismic motion simulation considering rupture process can be simplified as conventional seismic response numerical analysis for 3-dimentional site, the main difference is that incident wave used in site seismic response analysis is uniform excitation, but when considering the rupture process, input wave changes to the seismic motion field, which implies that the input waves for the boundary nodes of numerical calculation model are different.

ACKNOWLEDGEMENT

This research is supported by National Natural Science Foundation of China under grant no. 50978176.

REFERENCES

Miyatake, T. (1980). Numerical Simulations of earthquake source process by three-dimensional crack model, Part I, Rupture process. *J. Phys. Earth.* **28,**565-598.

Frankel, A. and Vidale, J. (1992). A three-dimensional simulation of seismic waves in the Santa Clara Valley,

California, from a Loma Prieta aftershock. *Bull. Seism. Soc. Am.* **82:5,** 2045-2074.
Frankel, A. (1993). Three-dimensional simulations of ground motions in the San Bernardino Valley, California, for hypothetical earthquakes on the San Andreas Fault. *Bull. Seism. Soc. Am.* **83:4,** 1020-1041.
Graves, R.W. (1993). Modeling three-dimensional site response effects in the Marina District basin, San Francisco, California. *Bull. Seism. Soc. Am.* **83:4,** 1042-1063.
Yomogida, K. and Etgen, J. T. (1993). 3-D wave propagation in the Los Angeles Basin for the Whittier-Narrows earthquake. *Bull. Seism. Soc. Am.* **83:5,** 1325-1344.
Olsen, K.B., Archuleta, R.J. and Matarese, J. R. (1995). Magnitude 7.7 earthquake on the San Andreas fault: three-dimensional ground motion in Los Angeles. *Science* **270,** 1628-1632.
Olsen, K.B. and Archuleta, R.J. (1996). 3-D simulation of earthquakes on the Los Angeles fault system. *Bull. Seism. Soc. Am.* **86:3,** 575-596.
Ohminato, T. and Chouet, B.A. (1997). A free-surface boundary condition for including 3D topography in the finite-difference method. *Bull. Seism. Soc. Am.* **87:2,** 494-515.
Pitarka, A., Irikura, K., Iwata, T. and Sekiguchi, H.(1998). Three-dimensional simulation of the near-fault ground motion for the 1995 Hyogoken Nanbu (Kobe), Japan, earthquake. *Bull. Seism. Soc. Am.* **88:2,** 428- 440.
Wald, D.J. and Graves, R.W. (1998). The seismic response of the Los Angeles Basin, California. *Bull. Seism. Soc. Am.* **88:2,** 337-356.
Aki, K. and Richards, P.G. (1980). Quantitative Seismology, Volume Ⅰ， W.H.Freeman, San Francisco,CA.
Liu Qi-Fang, JIN Xing, and DING Hai-Ping (2008). Effects of the Source Parameters on Long Period near-fault Ground Motion in the Case of Complex Site Condition. *Chinese Journal of Geophysics.* **51:1,**186-196. (in Chinese)
Xu Lisheng and Chen Yuntai (2002). Source time function and rupture process of earthquake. *Seismological and Geomagnetic Observation and Research.* **23:6,** 1-8.(in Chinese)
Anderson, J.G. and Richards, P.G. (1975). Comparison of strong ground motion from several dislocation models. *Geophys. J.R. Astr. Soc.*, **42:2,** 347～373
Liao ZP (2002). Introduction to Wave Motion Theories for Engineering, Second Edition, Science Press, Beijing, 190-213.